Structural evolution of a Ta-filament during hot-wire chemical vapour deposition of Silicon investigated by electron backscatter diffraction

C. J. Oliphant[1,2], C. J. Arendse[2,*], D. Knoesen[2], S. Prins[1] and G. F. Malgas[3]

[1] National Metrology Institute of South Africa, Private Bag X34, Lynwood Ridge, Pretoria 0040, South Africa

[2] Department of Physics, University of the Western Cape, Private Bag X17, Bellville 7535, South Africa

[3] CSIR National Centre for Nano-Structured Materials, P. O. Box 395, Pretoria 0001, South Africa

Abstract

In this study we investigate the structural changes of a burnt-out tantalum filament that was operated at typical hydrogenated nanocrystalline silicon synthesis conditions in our hot-wire chemical vapour deposition chamber. Scanning electron microscopy, energy dispersive X-ray spectroscopy, X-ray diffraction and for the first time electron backscatter diffraction showed that various silicides form preferentially along the length of the filament. At the cooler filament ends the $TaSi_2$ phase forms, encapsulating a Ta inner core. The tantalum rich Ta_5Si_3, Si_3Ta_5 and Ta_2Si phases however formed in addition to $TaSi_2$ at the centre regions. Cracks and porosity were found throughout the length of the filament. The microstructure evolution of the aged tantalum filament is discussed based on a model comprising hydrogen damage and the reactions between

* Corresponding author: C. J. Arendse, Tel: +27 21 959 3473, Fax: +27 21 959 3474,

Email: cjarendse@uwc.ac.za

the hot tantalum filament surface and silicon containing radicals. Possible effects of the well-known hydrogen treatment steps on filament degradation are also discussed.

Keywords: Hot-wire Chemical Vapour Deposition; Filament; Tantalum; electron backscatter diffraction; Silicides; Electron microscopy; Hydrogen damage; Energy Dispersive Spectroscopy, x-ray diffraction

1. Introduction

Filament ageing during the HWCVD of silicon thin films has been studied extensively [1-3]. Despite the remarkable progress in minimizing its influences on the filament operational lifetime [3-5] there still exists a need to further understand the filament ageing process, especially at nc-Si:H deposition conditions. Until recently, the only techniques used to characterize filament ageing has been limited to mostly x-ray diffraction (XRD), scanning electron microscopy (SEM), optical microscopy, in situ resistance/temperature curves and energy dispersive x-ray spectroscopy (EDS).

The electron backscatter diffraction (EBSD) technique is a microbeam based characterization tool that studies the crystallography of samples and is available to most modern electron microscopes. During a typical EBSD measurement the sample is tilted to an angle of ~ 70° relative to the incident electron beam in order to maximize the diffraction intensity. A high energy beam (≥ 20 kV) is then scanned over the specimen. Lines related to the spacing of crystal planes are then captured on a phosphor screen. These lines are referred to as Kikuchi patterns and they are characteristic to a given crystalline phase. Subsequently, software solves the Kikuchi patterns thereby

identifying the phase present at the area under investigation. Crystallographic information such as grain orientation, grain size, phases, misorientation, strain and texture can be acquired at a specific position on the sample. However, the detected EBSD signal originates from the first ~ 10 nm and sample preparation is therefore vital to obtain good quality Kikuchi pattern contrast [6]. In this study, we present EBSD measurements of a burnt-out Ta-filament that was used to synthesize nc-Si:H thin films. We then discuss the ageing process of the Ta-filament based on a model consisting of hydrogen damage and the reactions between the heated Ta-filament surface and Si containing radicals.

2. Experimental details

Ta-filaments with a diameter of ~ 300 μm and length 1 meter were used to synthesize nc-Si:H thin films using an MVSystems Inc HWCVD system described elsewhere [7]. Prior to and after each deposition, a standard H_2 gas treatment process was performed [4]. Cross-sections suitable for metallography of the burned-out Ta-filaments were prepared from the centre and end regions using fine grinding discs, polishing and then final polishing by means of ~ 40 nm colloidal silica suspension. The microstructure of the cross-sections were analysed using a field-emission gun scanning electron microscope (FEGSEM). Backscatter and forward scatter electron images were accumulated to discern the phases present. EDS was used to determine the relative elemental concentrations. The burned-out filament was also crushed along different sections for XRD studies. XRD spectra were collected in reflection geometry at 2θ-values ranging from 10 to 90° with a step size of 0.02°, using a PANaltyical XPert diffractometer operating at 45 kV and 40 mA. Copper Kα radiation with a wavelength of

1.5406 Å was used as the X-ray source. The XRD patterns were labelled using the database maintained by the International Centre for Diffraction Data (ICDD) [8].

3. Results

Fig. 1 shows a cross-section of the pure Ta-filament prior to the deposition. The different regions of contrast (Fig. 1a) is not due to differences in elemental composition but as a result of the orientation of the Ta grains with respect to the electron beam, illustrated by the EBSD grain map (Fig. 1b).

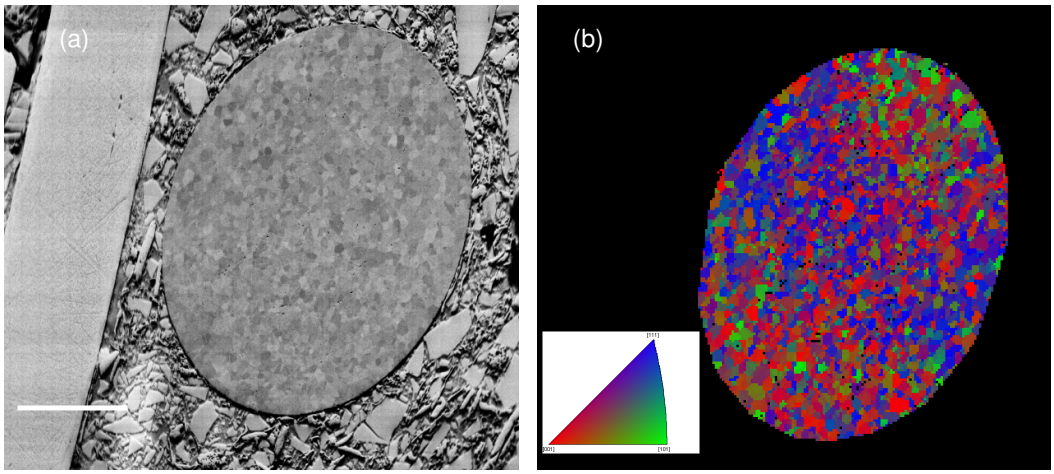

Fig. 1 (a) SEM micrographs of the pure Ta-filament and its (b) EBSD grain map with orientation key(inset).

Fig. 2 shows a cross-section of the filament taken from the ends at the contacts. The filament diameter increased by ~ 100 μm. Furthermore, the morphology changed drastically with a silicide layer (diameter ~ 250 μm) encapsulating a predominately Ta inner core (~ 150 μm in diameter) (Fig. 2a) [4]. Cracks appear within the silicide that extends throughout the length of the filament and it contains a porous structure (~ 50

μm thick) at its outer regions [2, 3]. Fig. 2b reveals that regions of contrast exist within the silicide layer and that they increase in length moving from the outer perimeter radially inwardly.

However, the EDS results taken from various points within the layer suggest that the elemental composition remains relatively constant throughout the silicide, i.e. ~ 73 at% Si and ~27 at% Ta, corresponding to a $TaSi_2$ phase [4]. This means that the contrast in the SEM micrograph is not caused by differences elemental composition. The inner core of the filament did not show as severe crack formation and is composed of ~ 20 at% Si and ~ 80 at% Ta.

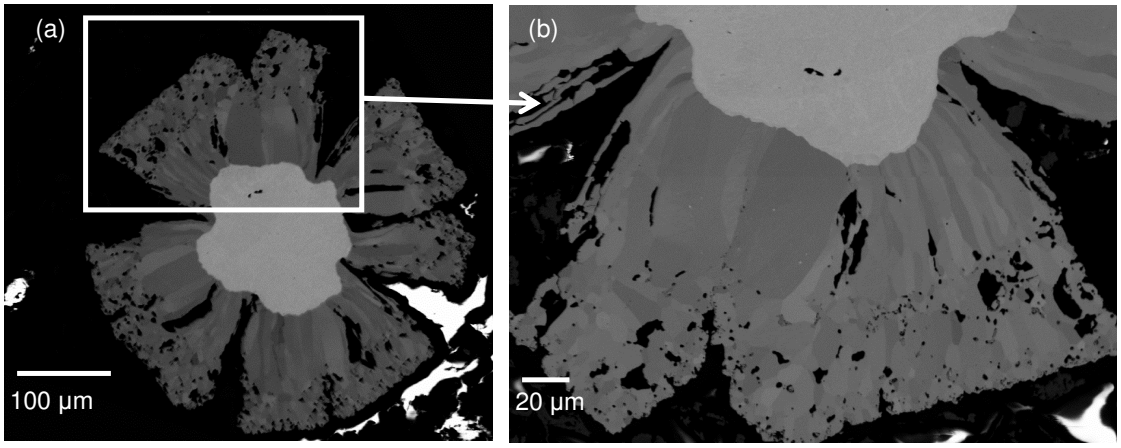

Fig. 2 (a) SEM micrograph of the filament cross-section sampled from the ends and (b) higher magnification micrograph.

Fig. 3 presents EBSD phase maps of the filament section shown in Fig. 2. The silicide present is the $TaSi_2$ phase, confirming the EDS analysis (Fig. 3a and its insets). The average grain size of the $TaSi_2$ phase increases inwardly from the outer perimeter (Fig 3b). These grains, and hence the electrons within the unit cell, are also orientated

differently (inset) with respect to the electron beam, which causes the contrast differences within the silicide layer observed in Fig. 2. The inner core appears to be composed of $TaSi_2$ and Ta, suggesting that the Ta was in the process of transforming into $TaSi_2$.

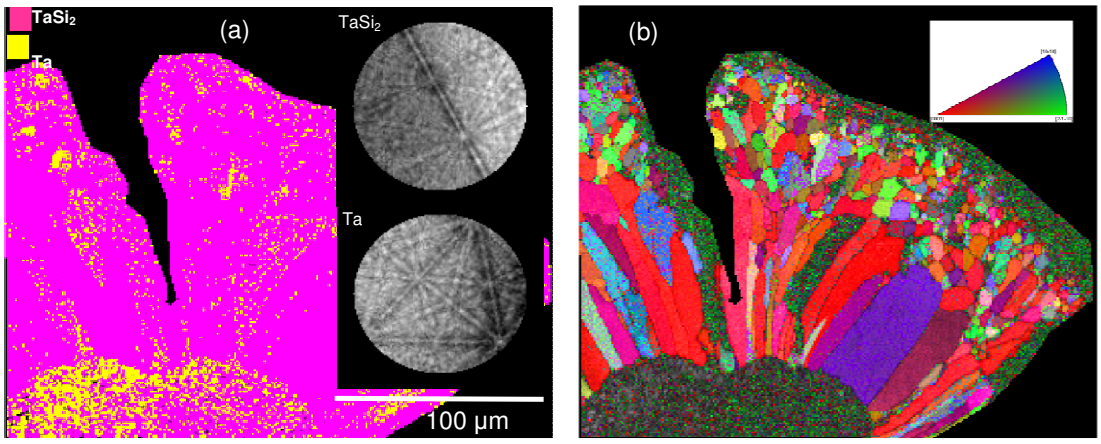

Fig. 3 (a) EBSD phase map of the filament cross-section at the ends and (b) the corresponding $TaSi_2$ grain map with orientation key (inset).

Fig. 4 shows SEM micrographs of the filament sampled from the centre region. The filament diameter increased slightly (~ 350 µm) compared to the end sections. Cracks and a ~ 60 µm thick porous structure are present, similar to the end regions. However, the porosity is enhanced and there appears to be at least 5 regions of different contrast (Fig. 4b). Table 1 shows the estimated Ta/Si concentrations. The Si content decreases while the Ta concentration increases radially inward. Regions A, B and C appear to possess similar elemental composition, which may suggest that these regions are actually one phase (possibly Ta_5Si_3) with a structure that varies radially inward. Regions D and E may be composed of a $TaSi_2$ phase and a Si containing Ta phase, respectively.

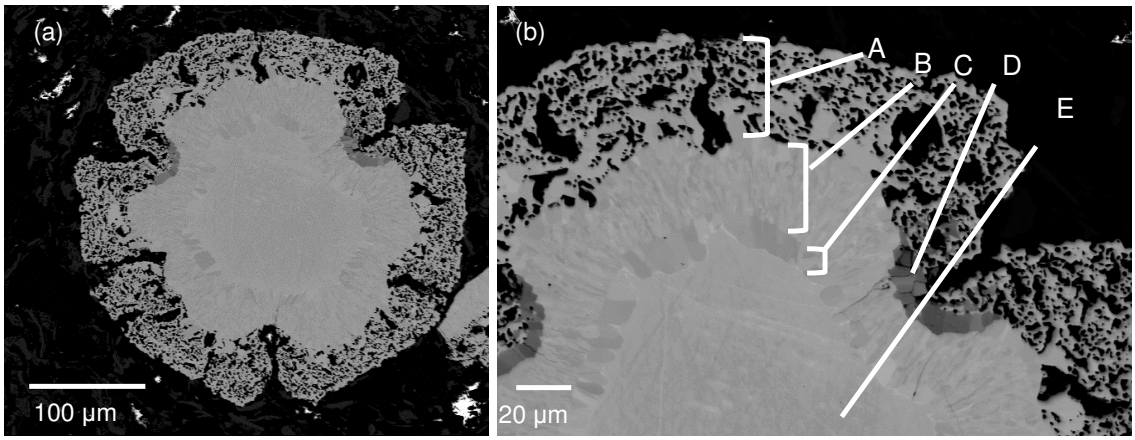

Fig. 4 (a) Cross-section of the filament sampled from the middle regions and (b) higher magnification micrograph revealing the different regions of contrast.

Table 1 EDS analysis of the Si and Ta concentrations of the regions of contrast A to E in Fig. 4.

Region	Ta (at%)	Si (at%)
A	50	50
B	52	48
C	53	47
D	26	74
E	79	21

Fig. 5 shows an EBSD phase map for the filament shown in Fig. 4. Contrary to the EDS results but complimentary to the backscatter images (Fig. 4b), 5 phases are identified and their sequence from the filament perimeter is $TaSi_2$ (region A and D), Ta_5Si_3 (region B), Si_3Ta_5 (region B), Ta_2Si (region C) and Ta (region E).

The reduction of the Si constituent within the silicides from the perimeter radially inward does however confirm the EDS analysis that there is a systematic decrease in the Si content radially inward.

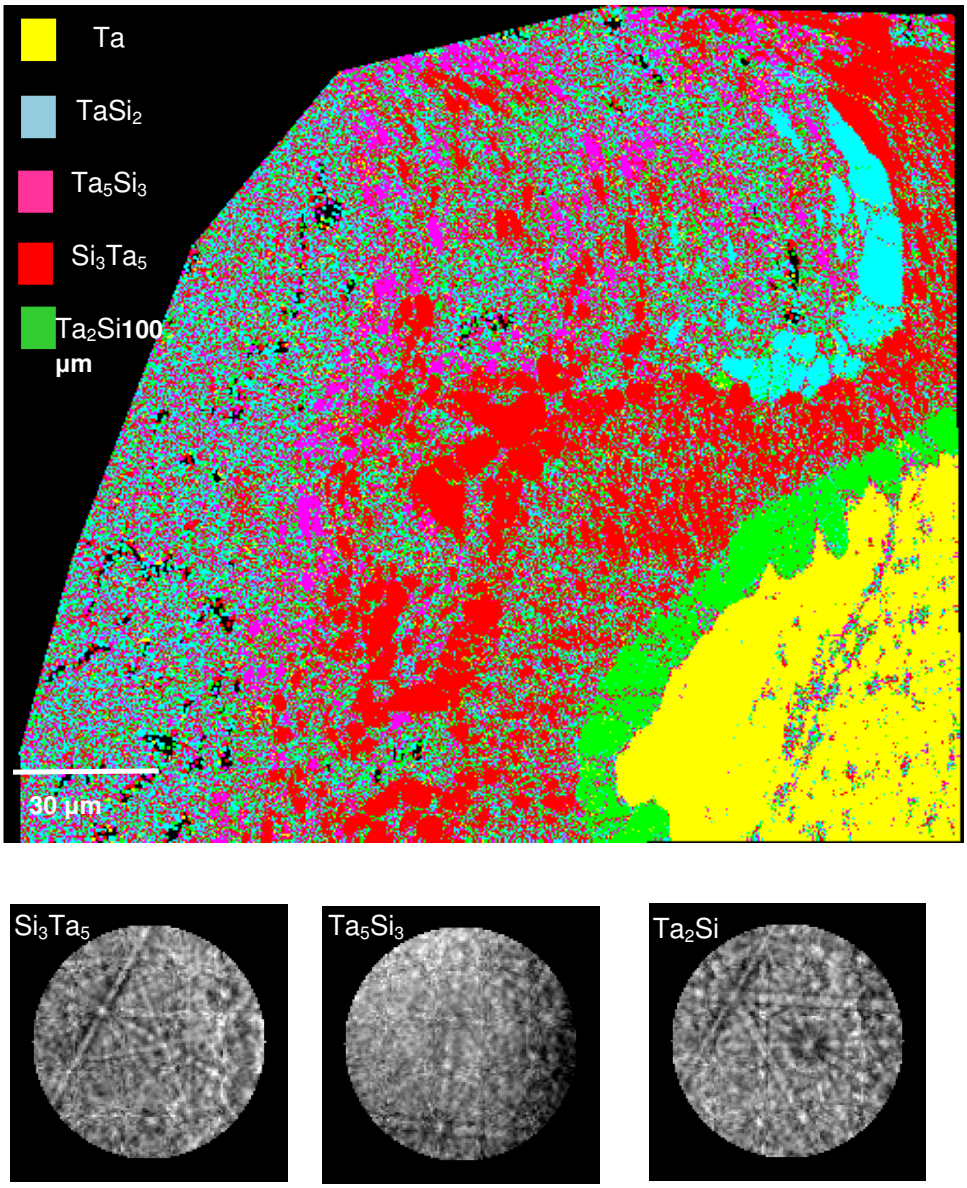

Fig. 5 EBSD phase map and Kikuchi patterns of the filament cross-section shown in Fig 4.

Fig. 6 shows the XRD patterns recorded on the pure Ta-filament and the crushed aged Ta-filaments. The XRD results compliments the SEM, EBSD and EDS results by disclosing that the pure Ta-filament transforms to various silicides, depending on the region of the filament itself. At the ends the silicon rich $TaSi_2$ forms and also Si were detected, whilst besides more Ta rich phases exist at the filament centre. The Si layer is easily disturbed from the filament, which maybe the reason why it was not observed at the filament cross-sections taken from the ends.

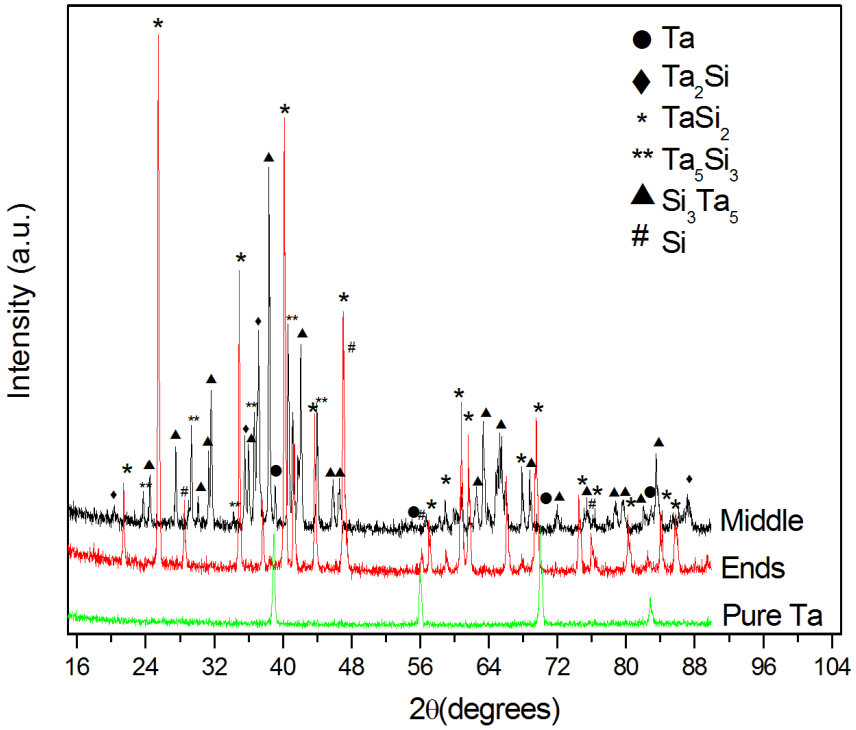

Fig. 6 XRD patterns of the pure Ta-filament and the crushed aged Ta-filaments.

4. Discussion

The reactions that occur between the SiH_4/H_2 precursor gas and the hot Ta surface are complex and include SiH_4 desorption, generation of adsorbed Si and H, Si diffusion on and into the filament, desorption of Si and H based radicals and even the formation of solid Si layers [3]. Nevertheless, we may deduce a filament ageing mechanism at nc-Si:H deposition conditions based on a model consisting of H-damage and reactions between Si-containing radicals and the filament surface.

The heated Ta-filament is an efficient decomposer of H_2 into atomic hydrogen [9] and SiH_4 into Si [10]. The generated Si based radicals may diffuse into the filament and at the right concentration relative to Ta at 1600 °C form Ta-silicides [11]. However, as the deposition time increases so does the silicide layer grows thicker, causing a reduction in the in-diffusion rate of Si to the Ta/Ta-silicide core [3,12]. This results in an accumulation of Si and consequently the formation of Si-rich silicides around the outer perimeter of the filament cross-sections and even some regions where there are a co-existence of different Ta-silicides.

The transformation of the Ta phase into the its silicides during the deposition of nc-Si:H thin films induces structural degradation in the form of cracks and a porous structure. These features are most likely caused by the differences in the mechanical properties of the Ta and the silicides such as the thermal expansion coefficient, hardness and brittleness [3 and references therein].

The thermal gradient along the filament itself introduces another factor that influences the filament degradation studies. Due to the high H_2 partial pressures used in nc-Si:H depositions as well as the hydrogen treatment steps [4], atomic and/or molecular hydrogen can diffuse into the filament. This in-diffusion of H-species may bring about structural degradation via hydrogen damage [13]. The recombination of atomic hydrogen into H_2 causes an increase in the pressure within the filament. This cause expansion and consequently crack formation. On the other hand, the evaporation of H_2 from the filament during cooling leads to the formation of pores and will be most severe at the surface of the filament. Another possibility is that atomic hydrogen may etch Si within the silicide layer, causing it to become porous at the surface of the filament. Ultimately, this leads to the observed increase of the average grain size of the silicides, such as the $TaSi_2$ phase, radially inward.

A possible reason for the observed enhanced Si concentration at the “cooler” filament ends may be accounted for by the reduced atomic hydrogen concentration and hence etching on Si, which enhances the Si accumulation at these regions. At the filament centre the higher temperature produces a higher concentration of atomic hydrogen, which reduces the Si content within and around the filament thereby promoting the formation of Ta rich silicides. Also, the desorption of Si from the filament surface may be enhanced at the “hotter” centre regions, also causing a reduction in Si and hence Ta rich silicides.

The results in this study show that in the case of nc-Si:H synthesis by HWCVD the hydrogen treatment process [4] may be detrimental to the filament lifetime. Other

means of extending the filament lifetime may therefore need to be explored, such as RF+DC filament heating [2] and/or heating the filament in a high vacuum [5].

5. Conclusion

Various microbeam analysis based investigations disclosed that a Ta-filament transforms into at least 4 different silicides during the deposition of nc-Si:H thin films by HWCVD. SEM, EBSD, EDS and XRD analysis concurred on the formation of the $TaSi_2$ phase around a Ta core at the filament ends while the Ta_2Si, Si_3Ta_5 and Ta_5Si_3 phases formed at the filament centre. The microstructural degradation and the preferential location of silicides were explained in terms of a model based on hydrogen damage and reactions between Si containing radicals and the heated Ta-filament. The possible detrimental effect that the hydrogen treatment steps could have on the filament lifetime was also identified.

Acknowledgements

The authors acknowledge the financial support of the National Research Foundation (NRF) and the National Metrology Institute of South Africa (Project no, TP021). The authors are especially thankful to Mr. David Motaung for the XRD measurements.

6. References

1. A.H. Mahan, A. Mason, B. P. Nelson, A.C. Gallagher, Mater. Res. Soc. Symp. Proc. 609 (2001) A6 (6.1).
2. D. Hrunski, B. Schroeder, M. Scheib, R. M. Merz, W. Bock, C. Wagner, Thin Solid Films 516 (2008) 818.
3. D. Hrunski, M. Scheib, M. Merz, B. Schroeder, Thin Solid Films 517 (2009) 3370.
4. D. Knoesen, C. Arendse, S. Halindintwali, T. Muller, Thin Solid Films 516 (2008) 814.
5. C.H.M. van der Werf, H. Li, V. Verlaan, C.J. Oliphant, R. Bakker, Z.S. Houweling, R.E.I. Schropp, Thin Solid Films 571 (2009) 3431.
6. J. Goldstein, D. Newbury, D. J. Joy, C. Lyman, P. Echlin, E. Lifshin, L. Sawyer, J. Michael, Scanning Electron Microscopy and X-ray Analysis 3rd edition, Kluwer Academic/Plenum Publishers (2003) 256.
7. C.J. Arendse, D. Knoesen, D.T. Britton, Thin Solid Films 501 (2006) 92.
8. Ta (00-001-1309), Ta_2Si (04-004-7298), $TaSi_2$ (00-008-0053), Si_3Ta_5 (04-004-7170), Ta_5Si_3 (04-004-8338) and Si (01-007-2109).
9. C. H. M. van der Werf, P. A. T. T. van Veenendaal, M. K. van Veen, A. J. Hardeman, M. Y. S. Rusche, J. K. Rath, R. E. I. Schropp, Thin Solid Films 430 (2003) 46.
10. R. E. I. Schropp, M. Zeman, Amorphous and microcrystalline silicon solar cells: modeling, materials, and device technology, Kluwer Academic Publishers (1998) 22.
11. A. Rockett, Materials science of semiconductors, Springer Science-Business Media (2007) 159.

12. E. Kolawa, J. S. Chen, J. S. Reid, P. J. Pokela, M. A. Nicolet, J. Appl. Phys. 70 (1991) 1369.

13. A. K. Das, Metallurgy of Failure Analysis, McGraw-Hill (1997) 132.